~400 μm into the reaction side to ensure that the reaction occurs in a homogenous concentration of ATP.

Fluorescent DNA–bead complexes were excited with the microscope's high-pressure mercury lamp using the appropriate filter set (blue filter set #11001; Chroma Technology, Brattleboro, VT). Fluorescence images were captured by a charge-coupled device camera (CCD-300T-IGF; Dage-MTI, Michigan City, IN) coupled to an image intensifier (VS4-1845; Video-Scope International, Sterling, VA), and were recorded on VHS videotape. To increase temperature to 37 °C, the microscope stage was enclosed in a Plexiglas housing and warm air was introduced.

DNA–bead preparation

The protocol used was modified from ref. 6. Bacteriophage λ DNA (0.096 pmoles; New England Biolabs) was biotinylated at one end by annealing and ligating a 3′-biotinylated, 12-mer oligonucleotide (50 pmoles; Operon Technologies) complementary to one of the cohesive ends. The biotinylated λ DNA ($3.6–7.2 \times 10^8$ molecules total) was reacted with 1 μm, streptavidin-coated, polystyrene beads (1.92×10^8 beads total; Bangs Laboratories) in 82 mM $NaHCO_3$ (pH 8.0) at 37 °C for 60 min. DNA–bead complexes were immediately transferred to a degassed solution containing 57 mM $NaHCO_3$ (pH 8.0), 30 mM dithiothreitol (DTT), 20% sucrose and 0.2 μM YOYO-1 (Molecular Probes). Dye binding was performed for a minimum of 60 min at 24 °C in the dark.

Single-molecule DNA helicase reactions

Before use, the flow cell was coated with either casein or BSA (100 μg ml^{-1}). The excess, unbound protein was washed out using 100 mM $NaHCO_3$ (pH 8.0). For each assay the sample syringe contained 41 mM $NaHCO_3$ buffer (pH 8.0), 35 mM DTT, 13% sucrose, 0.133 μM YOYO-1, 2 mM magnesium acetate, 1.92×10^8 DNA–bead complexes, and 4.6 nM RecBCD enzyme. The reaction syringe contained 41 mM $NaHCO_3$ buffer (pH 8.0), 35 mM DTT, 13% sucrose, 0.02 μM YOYO-1, 2 mM magnesium acetate, and ATP at the correct concentration. The *Escherichia coli* single-stranded DNA (ssDNA)-binding protein was not needed in these reactions because endonucleolytic cleavage of unwound ssDNA by the associated nuclease activity of RecBCD enzyme, releases the ssDNA as fragments that are immediately washed away in the buffer flow and, thus, do not accumulate to either inhibit the enzyme[19] or affect the observed fluorescence signal[7].

The RecBCD enzyme preparation used in all experiments was 100% active (data not shown) as determined using a spectrofluorometric helicase assay[11]. Standard visualization reactions were done at room temperature (~23 °C) using degassed buffers. Flow was initially at 0.8 ml h^{-1} for 10 min and was gradually decreased in increments of 50% to a final flow rate 10–20 μl h^{-1} (linear flow rates of ~80–150 μm s^{-1}), over a period of ~20 min.

Data analysis

Images were captured on a Power PC Macintosh computer interfaced with the VCR through an LG-3 frame-grabber card, operating at 1 frame per 33 ms, and controlled by Scion NIH Image v1.62c (Scion Corporation). Captured videos were converted into individual, time-stamped, sequential frames (Fig. 2) to make measurements. Individual DNA molecules were measured using the linear measurement tool of Scion NIH Image; calibration of the microscope optics was achieved using an Objective Micrometer (Fisher Scientific) that was marked in units of 10 μm.

The rate of DNA unwinding was calculated by measuring the observed length of DNA in each frame of a time course and fitting the resultant data to a linear function by least squares analysis. The resulting slope in each ATP-dependent reaction was corrected using the slope determined in the absence of ATP; this corrected slope was multiplied by the number of bp of λ DNA per μm to calculate the corrected rate in units of bp s^{-1}. Under the assay conditions used, the average length of individual, stretched, fluorescent λ DNA molecules was 14.9 μm (n = 43), which is shorter than previously published lengths[5,6]. Those reports used a higher concentration of sucrose and were done in the absence of magnesium ions. In our experiments, the length of a single, stretched λ DNA molecule was affected by flow rate and by the concentrations of sucrose, magnesium ions, and YOYO-1, varying from nore than 18 μm in 20% sucrose in the absence of magnesium acetate, to 14.9 μm in 13% sucrose and 2 mM magnesium acetate (data not shown). Thus, for all calculations, as λ DNA is 48,502 bp in length, and the observed average length of a λ DNA molecule is 14.9 μm, the average number of bp per μm is 48,502/14.9 = 3,255.

Received 23 May; accepted 23 October 2000.

1. Roman, L. J., Eggleston, A. K. & Kowalczykowski, S. C. Processivity of the DNA helicase activity of *Escherichia coli* recBCD enzyme. *J. Biol. Chem.* **267,** 4207–4214 (1992).
2. Arnold, D. A. & Kowalczykowski, S. C. in *Encyclopedia of Life Sciences* [online] (Nature Publishing Group, London, 1999) ⟨http:///www.els.net⟩.
3. Kowalczykowski, S. C., Dixon, D. A., Eggleston, A. K., Lauder, S. D. & Rehrauer, W. M. Biochemistry of homologous recombination in *Escherichia coli*. *Microbiol. Rev.* **58,** 401–465 (1994).
4. Kuzminov, A. Recombinational repair of DNA damage in *Escherichia coli* and bacteriophage lambda. *Microbiol. Mol. Biol. Rev.* **63,** 751–813 (1999).
5. Perkins, T. T., Smith, D. E. & Chu, S. Direct observation of tube-like motion of a single polymer chain. *Science* **264,** 819–822 (1994).
6. Brewer, L. R., Corzett, M. & Balhorn, R. Protamine-induced condensation and decondensation of the same DNA molecule. *Science* **286,** 120–123 (1999).
7. Eggleston, A. K., Rahim, N. A. & Kowalczykowski, S. C. A helicase assay based on the displacement of fluorescent, nucleic acid-binding ligands. *Nucleic Acids Res.* **24,** 1179–1186 (1996).
8. Ganesan, S. & Smith, G. R. Strand-specific binding to duplex DNA ends by the subunits of *Escherichia coli* recBCD enzyme. *J. Mol. Biol.* **229,** 67–78 (1993).
9. Bennink, M. L. *et al.* Single-molecule manipulation of double-stranded DNA using optical tweezers: interaction studies of DNA with RecA and YOYO-1. *Cytometry* **36,** 200–208 (1999).
10. Taylor, A. F. & Smith, G. R. Substrate specificity of the DNA unwinding activity of the RecBC enzyme of *Escherichia coli*. *J. Mol. Biol.* **185,** 431–443 (1985).
11. Roman, L. J. & Kowalczykowski, S. C. Characterization of the helicase activity of the *Escherichia coli* RecBCD enzyme using a novel helicase assay. *Biochemistry* **28,** 2863–2873 (1989).
12. Eggleston, A. K. & Kowalczykowski, S. C. The mutant recBCD enzyme, $recB^{2109}$CD enzyme, has helicase activity but does not promote efficient joint molecule formation *in vitro*. *J. Mol. Biol.* **231,** 621–633 (1993).
13. Taylor, A. & Smith, G. R. Unwinding and rewinding of DNA by the recBC enzyme. *Cell* **22,** 447–457 (1980).
14. Xue, Q. F. & Yeung, E. S. Differences in the chemical reactivity of individual molecules of an enzyme. *Nature* **373,** 681–683 (1995).
15. Wuite, G. J. L., Smith, S. B., Young, M., Keller, D. & Bustamante, C. Single-molecule studies of the effect of template tension on T7 DNA polymerase activity. *Nature* **404,** 103–106 (2000).
16. Roman, L. J. & Kowalczykowski, S. C. Characterization of the adenosinetriphosphatase activity of the *Escherichia coli* RecBCD enzyme: Relationship of ATP hydrolysis to the unwinding of duplex DNA. *Biochemistry* **28,** 2873–2881 (1989).
17. Bianco, P. R. & Kowalczykowski, S. C. Step size measurements on the translocation mechanism of the RecBC DNA helicase. *Nature* **405,** 368–372 (2000).
18. Zaitsev, E. N. & Kowalczykowski, S. C. Binding of double-stranded DNA by *Escherichia coli* RecA protein monitored by a fluorescent dye displacement assay. *Nucleic Acids Res.* **26,** 650–654 (1998).
19. Anderson, D. G. & Kowalczykowski, S. C. SSB protein controls RecBCD enzyme nuclease activity during unwinding: a new role for looped intermediates. *J. Mol. Biol.* **282,** 275–285 (1998).

Supplementary information is available on *Nature*'s World-Wide Web site (http://www.nature.com) or as paper copy from the London editorial office of *Nature*.

Acknowledgements

We would like to thank S. Chan and J. Lengyel for assistance with measurements, and the following people for their comments on the manuscript: N. Handa, J. Kleiman, A. Mazin, J. New, E. Seitz, M. Spies, T. Sugiyama and Y. Wu. This work was supported by an NIH Grant to S.C.K. and a DOE Center of Excellence for Laser Applications in Medicine Grant to Y.Y. and R.J.B.

Correspondence and requests for materials should be addressed to S.C.K. (e-mail: sckowalczykowski@ucdavis.edu).

Crystal structure of the transcription activator BmrR bound to DNA and a drug

Ekaterina E. Zheleznova Heldwein & Richard G. Brennan

Department of Biochemistry and Molecular Biology, Oregon Health Sciences University, Portland, Oregon 97201-3098, USA

The efflux of chemically diverse drugs by multidrug transporters that span the membrane[1] is one mechanism of multidrug resistance in bacteria. The concentrations of many of these transporters are controlled by transcription regulators, such as BmrR in *Bacillus subtilis*[2], EmrR in *Escherichia coli*[3] and QacR in *Staphylococcus aureus*[4]. These proteins promote transporter gene expression when they bind toxic compounds. BmrR activates transcription of the multidrug transporter gene, *bmr*, in response to cellular invasion by certain lipophilic cationic compounds (drugs)[2,5,6]. BmrR belongs to the MerR family, which regulates response to stress such as exposure to toxic compounds or oxygen radicals in bacteria[7–12]. MerR proteins have homologous amino-terminal DNA-binding domains but different carboxy-terminal domains, which enable them to bind specific 'coactivator' molecules. When bound to coactivator, MerR proteins upregulate transcription by reconfiguring the 19-base-pair spacer found between the −35 and −10 promoter elements to allow productive interaction with RNA polymerase[7,9–12]. Here we report the 3.0 Å resolution structure of BmrR in complex with the drug tetraphenylphosphonium (TPP) and a 22-base-pair oligodeoxynucleotide encompassing the *bmr* promoter. The structure reveals an unexpected mechanism for transcription activation that involves localized base-pair breaking, and base sliding and realignment of the −35 and −10 operator elements.

The structure of the BmrR–TPP–*bmr* promoter complex was determined by a combination of molecular replacement and multiple isomorphous replacement (Supplementary Information, Table 1). The asymmetric unit contains one BmrR monomer and a promoter half-site, which results in the statistical disorder of several base pairs of this pseudo-palindrome (Supplementary Information, Fig. 1). The monomer (Fig. 1a) contains three domains: the N-terminal DNA-binding domain (residues 1–75); the linker, containing an 11-turn α-helix, α5 (residues 76–119), that connects the N- and C-terminal domains; and the C-terminal drug-binding domain, the so-called BRC, (residues 120–278). The DNA-binding domain belongs to the superfamily of winged-helix proteins and contains a four-helix bundle and a three-stranded antiparallel β-sheet[13]. The topology is β1–α1–α2–β2–β3–α3–α4. Conserved hydrophobic core residues throughout the MerR family indicate that their DNA-binding domains assume similar folds (Supplementary Information, Fig. 2). The structure of the drug-binding domain, a distorted eight-stranded β-barrel, is identical to the previously solved structure of the individually expressed apo and TPP-bound BRC[14] (Supplementary Information).

The structure of dimeric BmrR bound to DNA resembles a butterfly (Fig. 1b). Each domain participates in dimerization, burying ~5,800 Å^2 of accessible surface area[15]. The DNA-binding domain of each monomer packs tightly against the drug-binding domain of its dimerization partner, and buries ~2,000 Å^2 of accessible surface area (ASA) per monomer (Fig. 1b, c). Helix α6 packs against helix α3′ and the C terminus of helix α1′, where the prime indicates the other subunit. In addition, the loop connecting strands β10 and β11 wedges between helices α3′ and α4′ of the DNA-binding domain. Linker helices α5 and α5′ bury ~900 Å^2 of ASA per monomer by forming an antiparallel coiled coil (Fig. 1b), which is likely to be found in all MerR family proteins[16]. Helix α5 also makes van der Waals contacts to helix α3′ and the loop between strands β10′ and β11′.

BmrR uses a helix–turn–helix (HTH) motif and two 'wings', W1 and W2, to bind the *bmr* promoter (Figs 1b and 2a). The HTH motif consists of helices α1 and α2, and the turn connecting them. Overlays of the 21-residue HTH domains of BmrR and of bacterial HTH proteins, PurR and TetR, as well as of bacterial winged-helix proteins, CAP and BirA, result in r.m.s. deviations of 0.9 Å, 1.1 Å, 1.2 Å and 1.2 Å, respectively. The symmetry-related recognition helices (residues 19–28) contact two consecutive major grooves whereby each helical axis is nearly perpendicular to the local DNA helical axis. Although helix α1 contributes a hydrogen bond from the amide of Gly 9 to the phosphate of cytosine 9′ and van der Waals contacts from the Cγ2 of Ile 8 to the deoxyribose ring of cytosine 9′, most HTH contacts are made by residues from helix α2 (Fig. 2). Hydrogen bonds occur between the amide of Ala 21 and guanine 4 phosphate, the NH2 and Nε of Arg23 and cytosine 8′ phosphate, and the Tyr 25 hydroxyl group and guanine 3 phosphate. van der Waals contacts include those between the NH2 of Arg 23 and the deoxyribose ring of cytosine 9′ and C7 atom of thymine 7′; the NH1 of Arg 23 and C7 atom of thymine 7′; and the Tyr 24 phenyl ring and C8 atom of adenine 2 and deoxyribose rings of guanine 3 and adenine 2 (Fig. 2b). Ser 18 and Lys 20 probably make DNA contacts, but their side chains are disordered.

The second DNA-binding element, wing W1, comprises strands β2 and β3 and their connecting loop (residues 35–46). Specifically, the hydroxyl group of Ser 41 makes hydrogen bonds to the cytosine 8′ phosphate, whereas that of Tyr 42 hydrogen bonds to the O4′ atom of the cytosine 9′ deoxyribose ring and the O2 of cytosine 10′, and makes van der Waals contacts to the guanine 10 N2. NH1, NH2 and the backbone amide of Arg 43 make hydrogen bonds to the phosphates of thymine 7′ and cytosine 8′ and a van der Waals contact to the cytosine 8′ deoxyribose ring. The Nε of Arg 43 makes a hydrogen bond to Oδ1 of Asp 26, which positions the Arg 43 side chain for reading the DNA (Fig. 2a). Arg 43 and a glutamate, aspartate or glutamine at position 26 are conserved in the MerR family indicating their importance in DNA binding by W1.

Unlike other winged-helix proteins[13], the third DNA-binding element of BmrR, wing W2, is not a loop, but rather another HTH motif composed of helices α3 and α4, and their connecting turn (Figs 1b and 2a). The α3 and α4 helices are less crossed than those of the major-groove binding HTH motif, and superimposition of their Cα atoms (residues 9–26 and 56–73) results in an r.m.s. deviation of 1.9 Å. The protein–DNA contacts made by W2 include hydrogen bonds between the Nε of Lys 60 and guanine 3 phosphate and the NH of Leu 66 and the adenine 2 phosphate. The dipole moment of helix α4 also contributes to binding as its electropositive N terminus points directly at the adenine 2 phosphate. Despite the large number of contacts between BmrR and its promoter, the DNA remains readily accessible for binding by RNA polymerase[7] (Fig. 1b).

The structure of the complex reveals no base-specific contacts. This might be due to the statistical disordering of the DNA or to potential specific contacts that are unresolved at the current resolution. BmrR might also achieve DNA recognition through

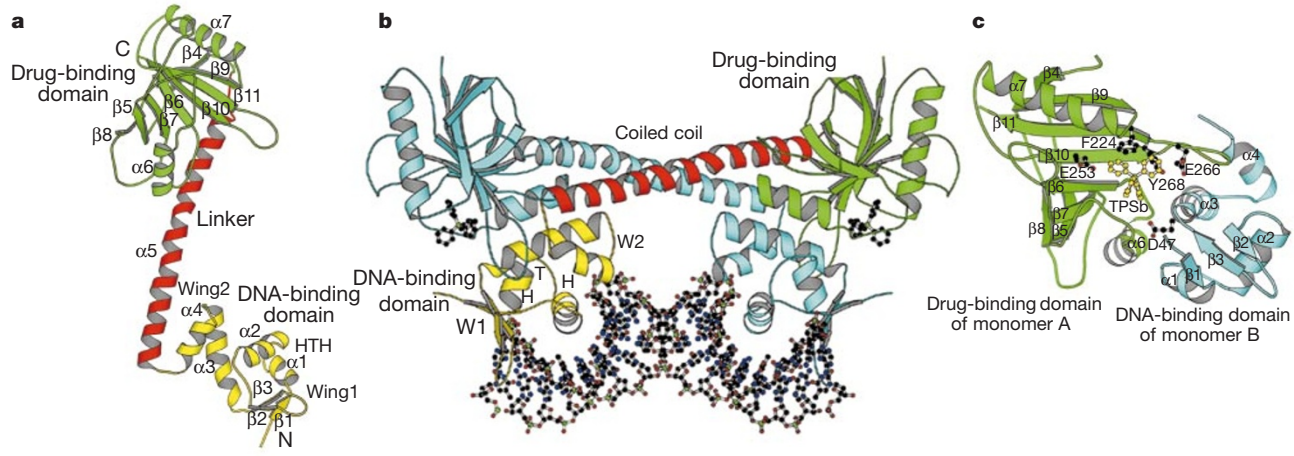

Figure 1 Crystal structure of the BmrR–drug–DNA complex. **a**, BmrR monomer. The DNA-binding domain, α-helical linker and drug-binding domain are shown in yellow, red and green, respectively. **b**, BmrR dimer bound to DNA. One monomer is coloured as in **a**, whereas the other monomer is shown in cyan. DNA and TPP/TPSb are represented as balls and sticks (carbon, black; nitrogen, blue; oxygen, red; and phosphorus/antimony, green). **c**, Dimerization interface between the drug-binding domain of a BmrR monomer (green) and the DNA-binding domain of its dimeric mate (cyan). The TPP/TPSb molecule and selected drug-binding residues are are represented as ball and sticks.

indirect readout. Alternatively, because BmrR is always bound to its promoter[2], perhaps only apo BmrR forms sequence-specific contacts with the *bmr* promoter. Drug binding would then enforce a different, high affinity protein–DNA interface characterized by the apparent lack of base-specific contacts.

The most striking feature of the BmrR–TPP–DNA complex is the DNA structure (Fig. 1b). Globally, the promoter is bent by ~50° at its middle towards the major groove and away from the protein; but many DNA-binding proteins bend and kink their operators. What makes the *bmr* promoter unique is the base-pair breaking and base sliding of the central base-pair step that is effected by the BmrR–TPP complex. In essence, the A·T base pairs that surround the pseudo dyad of the *bmr* promoter break, and the unpaired adenine and thymine slide away from each other towards the 3′ direction (Fig. 3a; and Supplementary Information, Fig. 1). Their final positions redefine the pseudo dyad of the promoter. Neither base participates in base pairing (Fig. 3a), and, because of the superimposition of the DNA and crystallographic dyads, adenine 1 and thymine 1 are related by a two-fold axis. This results in their statistical disorder and, owing to limited resolution of the data and the better fit of a pyrimidine to the electron density, both were refined as thymine 1. The bases at positions 2 and 2′, refined as adenine 2 and thymine 2′, also undergo displacement but still form a distorted Watson–Crick base pair. The presence of unpaired bases, immediately adjacent to the dyad axis, creates ripples on both strands whereby thymine 1 and adenine 2 on either strand are positioned against thymine 2′ on the opposite strand (Figs 2a and 3a; and Supplementary Information, Fig. 1).

The adjacent bases thymine 2′ and thymine 1 are unstacked, rolled out and undertwisted with rise, roll and helical twist values of 6.0 Å, 30° and 23°, respectively[17]. As a result, the operator 'bunches up' in the middle. The distorted DNA conformation is stabilized by interactions between residues Tyr 24, Tyr 25, Lys 60 and the N terminus of helix α4 with the phosphate backbone (Fig. 2a, b).

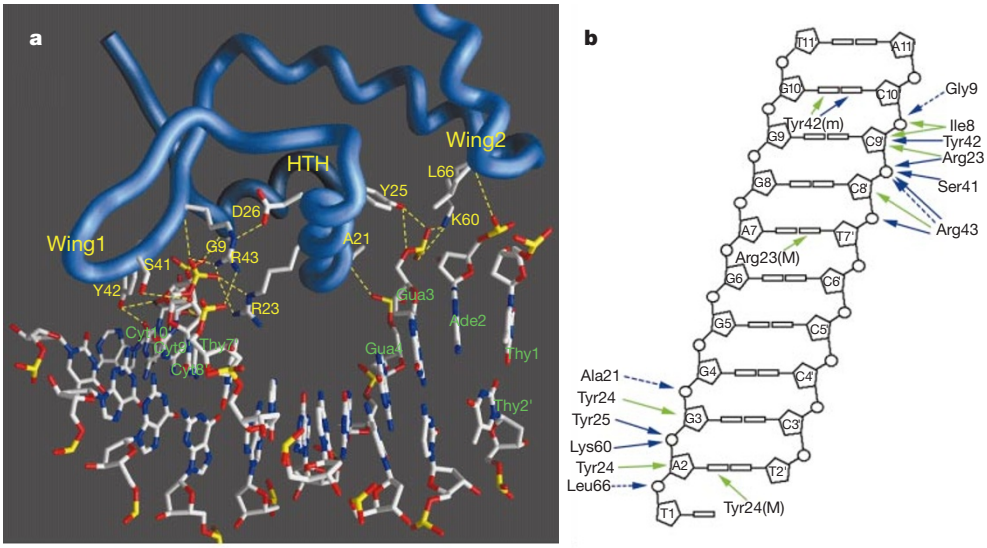

Figure 2 BmrR–DNA interactions. **a**, BmrR–DNA half-site interface. Atoms are represented as sticks (carbon, black; nitrogen, blue; oxygen, red; phosphorus, yellow). Hydrogen bonds are represented as yellow dashed lines. **b**, Representation of BmrR–DNA contacts. DNA is shown as a cylindrical projection where bases are depicted as rectangular boxes, deoxyribose rings as pentagons, and phosphates as circles. Hydrogen bonds are represented as blue, and van der Waals interactions as green arrows. Solid and dashed lines represent contacts from side chains and backbone amides, respectively. Side chains that contact bases in the major or minor grooves are labelled with 'M' and 'm', respectively.

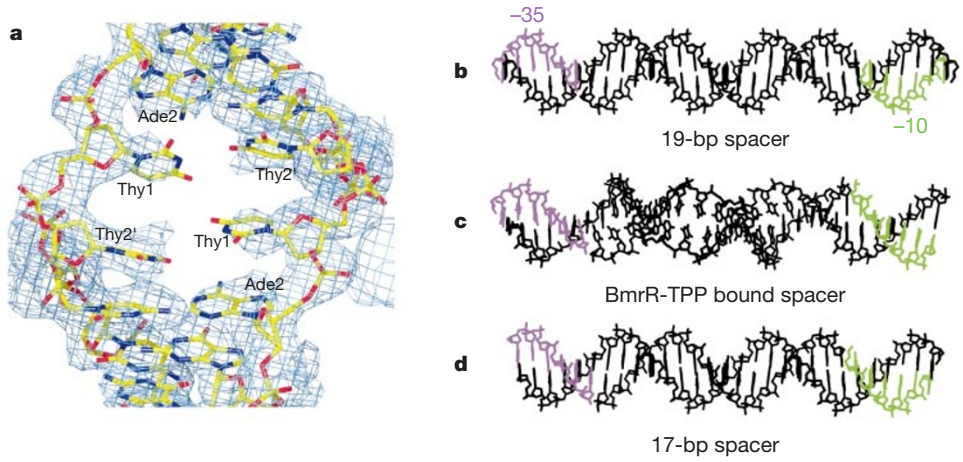

Figure 3 *bmr* promoter. **a**, The simulated-annealing omit electron density map at 1.0σ contour level, where Thy1, Thy2′ and Ade2, and all atoms within a 5 Å radius were deleted. DNA atoms are represented as sticks (carbon, yellow; nitrogen, blue; oxygen, red; phosphorus, yellow). **b**, Promoter with a 19-bp spacer. **c**, Promoter with a 19-bp spacer as observed in the BmrR–TPP bound operator. The full-length *bmr* promoter was modelled by adding 3-bp upstream and 7-bp downstream. **d**, Promoter with a 17-bp spacer. The –35 (TTGACT) and –10 (TACAGT) boxes of one strand are shown in pink and green, respectively.

A similar DNA structure is anticipated for all 'activated' MerR family members because each has a hydrogen-bond donor (lysine, arginine, glutamine) at position 60 and a completely conserved Tyr 25. Beyond this localized distortion, the remaining base pairs of the operator, 3/3′ to 11/11′, return to a duplex B-DNA like conformation with an average rise, roll and helical twist of 3.2 Å, 0.4°, and 32.0°, respectively. However, base pairs 6/6′ to 10/10′ are bent slightly (13°) towards the recognition helices (Figs 1b and 2a).

The mechanistic importance of the DNA distortion and altered conformation is underscored by previous biochemical studies on promoters regulated by MerR and SoxR, whereby deletion of 2 base pairs (bp) from their 19-bp spacers resulted in regulator-independent promoters[18,19]. In a canonical B-DNA conformation, a 19-bp spacer places the −35 and −10 elements of the *bmr* promoter onto opposite sides of the DNA double helix, thereby preventing RNA polymerase from productively accessing both elements simultaneously (Fig. 3b). In contrast, a 17-bp spacer in the B-DNA conformation brings the −35 and −10 promoter elements onto the same side of the DNA (Fig. 3d). This spacer-length is found in most σ^A-regulated promoters. The result of the BmrR–TPP-induced base unpairing and sliding is to shorten the DNA by ~5 Å, or about 2 bp, compared to the end-to-end length of a 21-bp B-DNA. More importantly, the local untwisting of the DNA brings the −35 and −10 promoter elements onto the same face of the DNA double helix; much like the transcription-ready 17-bp spacer does (Fig. 3c, d).

To restructure the *bmr* promoter, DNA-bound BmrR must bind a coactivator—one of several structurally unrelated lipophilic cations, such as TPP[2,5]. The present structure includes a molecule of tetraphenylantimonium (TPSb), a tetraphenylphosphonium analogue (Supplementary Information, Table 1). The drug-binding pocket is created primarily by residues from the drug-binding domain, with an unanticipated contribution from the DNA-binding domain (Fig. 1c). The phenyl rings of the TPSb molecule make van der Waals and stacking interactions with the side chains of residues Phe 224 and Tyr 268. Complementary electrostatic interactions are found between the TPSb molecule and carboxylate groups of Asp 47, Glu 253 and Glu 266 (Fig. 1c), and backbone carbonyl oxygens of loop residues Pro 144, Glu 145 and Asn 146. This binding mode, based on electrostatic, stereochemical and steric complementarity between the drug and the drug-binding pocket, is similar to that observed in the BRC–TPP structure[14]. However, the roles of Asp 47 and Glu 266 are unclear because BRC, which lacks Asp 47, and BmrR bind the same drugs with equal affinities[5]. Moreover, in the structure of the BRC–TPP complex, Glu 266 is disordered with only Glu 253 contributing to drug–protein charge complementarity.

In the absence of the structure of the apo BmrR–DNA complex, how drug binding is coupled to DNA distortion and transcription activation is unclear. Superimposition of residues 121–277 of the apo BRC and TPP-bound BmrR structures suggests that helix α6 of the drug-binding domain repacks against helix α3′ of the DNA-binding domain as a key part of the signalling mechanism. This repacking will clearly also impinge on helices α4′ and α5 (Fig. 1b). The signal of drug binding could be then transmitted in two ways: directly, toward the protein–DNA interface; and allosterically, towards the protein–DNA interface of the other subunit through the coiled coil, the latter of which is supported by mutational studies on MerR[16,20].

The structure of the BmrR–TPP–DNA complex provides an excellent model for understanding transcriptional regulation by other MerR family proteins. For example, the Hg^{2+}-binding residues of MerR[21] can be placed at the N terminus of helix α5 (Cys 82), near the C terminus of helix α5′ (Cys 117), and on a nearby loop (Cys 126), thus bringing their sulphydryls into proximity for facile trigonal coordination of Hg^{2+}. Activation-deficient mutants of SoxR, which binds 2Fe–2S redox centres, map to four cysteines of the C-terminal portion of α5 and slightly beyond[22] (Supplementary Information, Fig. 2). The constitutively active MerR mutants S86C and A89V can be rationalized[16,20] as the result of a readily formed Cys 86/Cys 117 disulphide bond or new van der Waals interactions between A89V and its hydrophobic neighbours. Both would lock the apo protein into the activated form. Other constitutively active MerR phenotypes[16] map to helices α3 and α5, and again can be explained readily by hydrogen bonds or van der Waals interactions that favour the activated conformation of the protein. By contrast, the activation-deficient MerR mutant[7], A60V, would sterically prohibit the packing of helices α3′ and α4′ of the Hg^{2+}-bound protein. The locations of these mutations underscore the critical role of the α3′/α4′/α5 interfaces in transcription regulation by the MerR family. □

Methods

Sample preparation and crystallization

The C-terminal His-tagged *bmrR* gene, subcloned into the pBAD plasmid under control of an arabinose-inducible promoter, was kindly provided by P. N. Markham and A. A. Neyfakh (University of Illinois, Chicago, Illinois). *E. coli* Top10 cells were transformed with this vector, grown at 37 °C to an absorbance at 595 nm of 0.6–0.8, and induced with 0.03% D-arabinose. After a 3-h induction, the cells were pelleted and lysed using a French press. BmrR was purified by Ni-NTA column chromatography and eluted with 400 mM imidazole. BmrR is poorly soluble and precipitates immediately after elution; however, the protein was resolubilized by adding a 22-bp DNA duplex encompassing the *bmr* operator sequence with a 5′ A or T overhang (Supplementary Information, Fig. 1a). The BmrR–DNA mixture was dialysed against 20 mM Tris-HCl, pH 7.6, 0.2 M NaCl and 10% glycerol, and concentrated to 5–8 mg ml^{-1}. TPP, dissolved in dimethyl sulphoxide (DMSO), was added to the BmrR–DNA mixture to final concentrations of 5 mM TPP and 1% DMSO. Crystals of the ternary complex were grown at room temperature by the hanging-drop vapour-diffusion method against reservoirs containing 1.0–1.2 M imidazole, pH 6.5.

Data collection and structure determination

X-ray intensity data for the BmrR–TPP–DNA complex were collected at room temperature with an R-AXIS IV imaging plate system, mounted on a Rigaku RU300 X-ray generator equipped with Yale focusing mirrors, and processed using BIOTEX (Molecular Structure Corporation, Woodlands, Texas). The crystals took the tetragonal space group $P4_{1/3}22$ with unit-cell dimensions: $a = b = 109.5$ Å, $c = 144.3$ Å, $\alpha = \beta = \gamma = 90°$. The structure of the BmrR–TPP–DNA complex was solved by a combination of molecular replacement[23] and multiple isomorphous replacement[24]. Heavy atom derivatives were prepared by soaking native crystals in solutions of K_2PtCl_4 or thimerosal, and by crystallizing the complex with 5-iodouridine-containing DNA (Supplementary Information, Fig. 1c). Initially, the location of the BRC domain was determined by molecular replacement using data in the resolution range 15.0–4.0 Å and the entire apo BRC monomer as a search model. Only space group $P4_322$ yielded a correct solution, which had a correlation coefficient of 45.2% and an R_{factor} of 51.9%.

Because no connected density was observed for the N-terminal domain or the DNA, phases were calculated from the molecular replacement solution to locate the single iodine site in the Iodo1 derivative. This allowed the identification of one platinum and one mercury site in subsequent cross-difference Fourier analyses. The heavy atom parameters (Supplementary Information) were refined by the maximum-likelihood method to 3.0 Å resolution[24]. A solvent-flattened map (78% estimated solvent) revealed the density for the DNA-binding domain and the α-helical linker. A polyalanine model was built to the density using O[25]. Phase combination[24] showed clear density for most of the BmrR residues and the DNA phosphate backbone. Intensity data sets were also collected on crystals of BmrR complexes in which the DNA contained 5-iodouridine at positions 2′, 7′, 1 and 9′, referred to as complexes Iodo2, Iodo3, Iodo5 and Iodo6, respectively (Supplementary Information, Fig. 1). These data allowed the correct base assignment of the DNA sequence.

Before refinement, 5% of all data were set aside for cross-validation[26]. Through iterative cycles of refinement with TNT[27] and model rebuilding[25], residues 3–277 and the DNA were built. A metal ion coordinated by His 189 was refined as a Zn^{2+} ion at occupancy of 0.5. The final model was verified by a series of $F_o - F_c$ omit and simulated annealing omit electron density maps. Residues 1–2, 278, the six histidines of the C-terminal His-tag, and the DNA 5′-overhangs are disordered and not included in the final model. Forty-five amino-acid residues were refined as alanines because their side-chain density is either poor or missing. The final model has no Ramachandran outliers, as assessed by the program PROCHECK[28] (Supplementary Information, Table 1). The secondary structure elements were assigned by PROCHECK[28] and include β-strands β1 (residues 5–7), β2 (residues 34–36), β3 (43–46), β4 (124–128), β5 (133–138), β6 (170–174), β7 (189–193), β8 (208–211), β9 (216–223), β10 (248–257) and β11 (268–276), and α-helices α1 (8–14), α2 (19–28), α3 (48–62), α4 (66–74), α5 (77–116), α6 (153–163) and α7 (226–242). Because of the poor density of the TPP molecule, isomorphous crystals of BmrR–TPSb–DNA complex were obtained by soaking TPSb into crystals of BmrR–TPP–DNA complex. The resulting difference electron-density map revealed the density for the entire drug. The BmrR–TPSb–DNA complex was refined with TNT[27].

Figures were prepared using MOLSCRIPT[29], GRASP[15] and O[25].

Received 15 September; accepted 6 November 2000.

1. Saier, M. H. Jr *et al.* Evolutionary origins of multidrug and drug-specific efflux pumps in bacteria. *FASEB J.* **12,** 265–274 (1998).
2. Ahmed, M., Borsch, C. M., Taylor, S. S., Vazques-Laslop, N. & Neyfakh, A. A. A protein that activates expression of a multidrug efflux transporter upon binding the transporter substrates. *J. Biol. Chem.* **269,** 28506–28513 (1994).
3. Broun, A., Tomashek, J. J. & Lewis, K. Purification and ligand binding of EmrR, a regulator of a multidrug transporter. *J. Bacteriol.* **181,** 5131–5133 (1999).
4. Grkovic, S., Brown, M. H., Roberts, N. J., Paulsen, I. T. & Skurray, R. A. QacR is a repressor protein that regulates expression of the *Staphylococcus aureus* multidrug efflux pump QacA. *J. Biol. Chem.* **273,** 18665–18673 (1998).
5. Markham, P. N., LoGuidice, J. & Neyfakh, A. A. Broad ligand specificity of the transcriptional regulator of the *Bacillus subtilis* multidrug transporter Bmr. *Biochem. Biophys. Res. Commun.* **239,** 269–272 (1997).
6. Vazquez-Laslop, N., Markham, P. N. & Neyfakh, A. A. Mechanism of ligand recognition by BmrR, the multidrug-responding transcriptional regulator: mutational analysis of the ligand-binding site. *Biochemistry* **38,** 16925–16931 (1999).
7. Summers, A. O. Untwist and shout: a heavy metal-responsive transcriptional regulator. *J. Bacteriol.* **174,** 3097–3101 (1992).
8. Holmes, D. J., Caso, J. L. & Thompson, C. J. Autogenous transcriptional activation of a thiostrepton-induced gene in *Streptomyces lividans*. *EMBO J.* **12,** 3183–3191 (1993).
9. Ansari, A. Z., Bradner, J. E. & O'Halloran, T. V. DNA-bend modulation in a repressor-to-activator switching mechanism. *Nature* **374,** 371–375 (1995).
10. Gaudu, P. & Weiss, B. SoxR, a [2Fe-2S] transcription factor, is active only in its oxidized form. *Proc. Natl Acad. Sci. USA.* **93,** 10094–10098 (1996).
11. Hidalgo, E., Ding, H. & Demple, B. Redox signal transduction via iron-sulfur clusters in the SoxR transcription activator. *Trends Biochem. Sci.* **22,** 207–210 (1997).
12. Outten, C. E., Outten, F. W. & O'Halloran, T. V. DNA distortion mechanism for transcriptional activation by ZntR, a Zn(II)-responsive MerR homologue in *Escherichia coli*. *J. Biol. Chem.* **274,** 37517–37524 (1999).
13. Gajiwala, K. S. & Burley, S. K. Winged helix proteins. *Curr. Opin. Struct. Biol.* **10,** 110–116 (2000).
14. Zheleznova, E. E., Markham, P. N., Neyfakh, A. A. & Brennan, R. G. Structural basis of multidrug recognition by BmrR, a transcription activator of a multidrug transporter. *Cell* **96,** 353–362 (1999).
15. Honig, B. & Nicholls, A. Classical electrostatics in biology and chemistry. *Science* **268,** 1144–1149 (1995).
16. Caguiat, J. J., Watson, A. L. & Summers, A. O. Cd(II)-responsive and constitutive mutants implicate a novel domain in MerR. *J. Bacteriol.* **181,** 3462–3471 (1999).
17. Lavery, R. & Sklenar, H. Defining the structure of irregular nucleic acids: conventions and principles. *J. Biomol. Struct. Dyn.* **6,** 655–667 (1989).
18. Parkhill, J. & Brown, N. L. Site-specific insertion and deletion mutants in the *mer* promoter-operator region of Tn501; the nineteen base-pair spacer is essential for normal induction of the promoter by MerR. *Nucleic Acids Res.* **18,** 5157–5162 (1990).
19. Hidalgo, E. & Demple, B. Spacing of promoter elements regulates the basal expression of the *soxS* gene and converts SoxR from a transcriptional activator into a repressor. *EMBO J.* **16,** 1056–1065 (1997).
20. Comess, K. M., Shewchuk, L. M., Ivanetich, K. & Walsh, C. T. Construction of a synthetic gene for the metalloregulatory protein MerR and analysis of regionally mutated proteins for transcriptional regulation. *Biochemistry* **33,** 4175–4186 (1994).
21. Zeng, Q., Stalhandske, C., Anderson, M. C., Scott, R. A. & Summers, A. O. The core metal-recognition domain of MerR. *Biochemistry* **37,** 15885–15895 (1998).
22. Bradley, T. M., Hidalgo, E., Leautaud, V., Ding, H. & Demple, B. Cysteine-to-alanine replacements in the Escherichia coli SoxR protein and the role of the [2Fe-2S] centers in transcriptional activation. *Nucleic Acids Res.* **25,** 1469–1475 (1997).
23. Kissinger, C. R., Gehlhaar, D. K. & Fogel, D. B. Rapid automated molecular replacement by evolutionary search. *Acta Crystallogr. D* **55,** 484–491 (1999).
24. Furey, W. & Swaminathan, S. PHASES-95: a program package for the processing and analysis of diffraction data from macromolecules. *Methods Enzymol.* **277B,** 590–620 (1997).
25. Jones, T. Z., Zou, J. -Y., Cowan, S. W. & Kjeldgaard, M. Improved methods for building protein models in electron density maps and the location of errors in these models. *Acta Crystallogr. A* **47,** 110–119 (1991).
26. Brünger, A. T. Free R value: cross-validation in crystallography. *Methods Enzymol.* **277B,** 366–396 (1997).
27. Tronrud, D. E. TNT refinement package. *Methods Enzymol.* **277B,** 306–319 (1997).
28. Laskowski, R. A., MacArthur, M. W. & Thornton, J. M. PROCHECK: a program to check the stereochemical quality of protein structures. *J. Appl. Crystallogr.* **26,** 283–291 (1993).
29. Kraulis, P. J. MOLSCRIPT: a program to produce both detailed and schematic plots of protein structures. *J. Appl. Crystallogr.* **24,** 946–950 (1991).

Supplementary information is available on *Nature*'s World-Wide Web site (http://www.nature.com) or as paper copy from the London editorial office of *Nature*.

Acknowledgements

The authors thank P. N. Markham and A. A. Neyfakh for providing the *bmrR* expression construct and for helpful comments. This research was supported by the NSF, NIH and the Medical Research Foundation of Oregon (R.G.B.) and the American Heart Association (E.E.Z.H.).

Correspondence and requests for materials should be addressed to R.G.B. (e-mail: brennanr@ohsu.edu). Coordinates for the BmrR–TPP–DNA and BmrR–TPSb–DNA complexes have been deposited in the RCSB Protein database under accession code *1exj* and *1exi*, respectively.

correction

Halocarbons produced by natural oxidation processes during degradation of organic matter

F. Keppler, R. Eiden, V. Niedan, J. Pracht & H. F. Schöler

Nature **403,** 298–301 (2000).

Throughout Figs 2–4 and the corresponding legends, mM should have been mmol, μM should have been μmol, and pM should have been pmol. In addition, in Fig. 3a the *x* axis should have been labelled 'Fe (II) conc. in medium (μmol)'; and in Fig. 3b the *x* axis should have been labelled 'Halide ion conc. in medium (mmol)'. □

erratum

Memory B-cell persistence is independent of persisting immunizing antigen

Mitsuo Maruyama, Kong-Peng Lam & Klaus Rajewsky

Nature **407,** 636–642 (2000).

In this paper, Table 1 was printed incorrectly. It should have appeared as below. □

Table 1 *in vitro* secondary antibody responses of PE^+IgG1^+ memory B cells

		Antibodies ($\mu g\,ml^{-1}$)					
		Anti-PE			Anti-NP		
Memory B cells	$CD4^+$ T cells	IgG1	IgM	Igλ	IgG1	IgM	Igλ
PE^+NP^-	PE primed	34.1±1.0	<0.1	33.7±0.1	<0.1	<0.1	<0.1
PE^+NP^-	NP/CG primed	<0.1	<0.1	<0.1	<0.1	<0.1	<0.1
NP^+PE^-	PE primed	<0.1	<0.1	<0.1	<0.1	<0.1	<0.1

Numbers represent the concentration of anti-PE or anti-NP antibody (in $\mu g\,ml^{-1}$). Titres were obtained from three independent wells and the mean ± s.e.m. is shown.